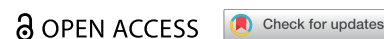


RESEARCH ARTICLE



# Multi-functional chitosan copolymer modified nanocrystals as oral andrographolide delivery systems for enhanced bioavailability and anti-inflammatory efficacy

Wan Liu<sup>a,#</sup>, Meng Cheng<sup>a,b,#</sup>, Zhiyang Lu<sup>a</sup>, Haocheng Li<sup>a</sup>, Yulin Feng<sup>a</sup>, Yi Jin<sup>a</sup>, Shilin Yang<sup>a</sup>, Jianfang Feng<sup>a,c</sup> and Liangxing Tu<sup>a</sup>

<sup>a</sup>National Pharmaceutical Engineering Center for Solid Preparation in Chinese Herbal Medicine, Jiangxi University of Chinese Medicine, Nanchang, China; <sup>b</sup>The Affiliated Hospital, Jiangxi University of Chinese Medicine, Nanchang, China; <sup>c</sup>School of Pharmacy, Guangxi University of Chinese Medicine, Nanning, China

## ABSTRACT

Modifying nanocrystals with functional materials have been common strategy to enlarge the enhancing ability on oral absorption via nanocrystals; however, whether the functional materials have played their full enhancing ability in oral absorption is still unknown. In this study, we synthesized a novel chitosan-based copolymer (the copolymer of sodium dodecyl sulfate (SDS), chitosan (CS) and D- $\alpha$ -Tocopherol polyethylene glycol 1000 succinate, SDS-CS-TPGS), and modified nanocrystals with this copolymer, aiming to enhance the oral absorption of polymer andrographolide (ADR). In real-time distribution study, we found the distribution of ADR, SDS, CS and TPGS varies in gastrointestinal tract, while the distribution of ADR and SDS-CS-TPGS was similar, revealing the SDS-CS-TPGS could able to participate in the absorption process of andrographolide timely. To explore the oral absorption enhancing ability of SDS-CS-TPGS, we prepared a series of nanocrystals modified with different materials and explored their pharmacokinetic performances on SD rats. The results showed the nanocrystals modified with SDS-CS-TPGS (S-C-TANs) exhibited the highest bioavailability, which could enhance the  $AUC_{0-\infty}$  of ADR from 1.291 mg/L\*h to 5.275 mg/L\*h (enhanced for about 4.09-folds). The enhanced anti-inflammatory efficacy was also found on ICR mice by employing ear swelling rate, TNF- $\alpha$ , IL-1 $\beta$  and IL-6 and pharmacodynamic index. These results indicated that modified with synthesized copolymer containing different functional stabilizers is an efficient strategy to enlarge the enhancing ability on oral absorption of nanocrystals.

## ARTICLE HISTORY

Received 26 August 2022  
Revised 14 November 2022  
Accepted 15 November 2022





## KEYWORDS

Andrographolide; chitosan; bioavailability; real-time distribution; anti-inflammatory


## 1. Introduction

Inflammation and inflammation related diseases are threatening the health of human beings (He et al., 2020; Methenitis et al., 2021), and andrographolide, one of the major diterpenoid extracted from *ANDROGRAPHIS PANICULATA*, is widely used as an anti-inflammatory reagent in China (Tran et al., 2020; Magar et al., 2023). The modern pharmacological studies showed andrographolide has a variety of pharmacological activities, for example anti-inflammatory (Hussain et al., 2022), anti-cancer (Khan et al., 2018), anti-oxidative effects (Wang et al., 2021), anti-thrombosis (Li et al., 2021), inhibiting virus (Latif & Wang, 2020), anti-asthma (Lim et al., 2021), and anti-bacteria (Zhang et al., 2021). However, the clinical application of andrographolide is limited because of its poor water solubility and low bioavailability (Casamonti et al., 2019), and how to improve the oral bioavailability of poor soluble drugs like andrographolide has become a research focus in pharmaceutical field (Zafar et al., 2021).

Nano delivery system has been a popular route to enhance the bioavailability of poor soluble drugs (Marta et al., 2019). To date, researchers have employed multiple nanotechnologies to enhance the oral bioavailability of andrographolide, such as nanoemulsion (Zou et al., 2022), nanoparticles (Chellampillai & Pawar 2011; Parveen et al., 2014), micelles (Zhang et al., 2014), and nanocrystals (Basu et al., 2020). Among these nanotechnologies, nanocrystal technology is more popular due to its advantages like high drug loading, easy preparation and no special requirement for physical-chemical properties of drugs (Zhao et al., 2020; Cheng et al., 2020). In general, nanocrystals enhance the oral absorption of drugs mainly by increasing their saturation solubilities and dissolution rates caused by the decreased particle sizes of nanocrystals (Kesisoglou et al., 2007; Tu et al., 2020). Nanocrystal technology has shown its huge success on oral formulation as there are nearly ten products based on nanocrystals approved by FDA (Lu et al., 2015; Liu et al.,

**CONTACT** Liangxing Tu  [tufrankie@163.com](mailto:tufrankie@163.com)  National Pharmaceutical Engineering Center for Solid Preparation in Chinese Herbal Medicine, Jiangxi University of Chinese Medicine, Nanchang, 330006, China; Jianfang Feng  [fengjianfang@vip.163.com](mailto:fengjianfang@vip.163.com)  National Pharmaceutical Engineering Center for Solid Preparation in Chinese Herbal Medicine, Jiangxi University of Chinese Medicine, Nanchang, 330006, China

<sup>#</sup>These two authors contributed equally to this work.

 Supplemental data for this article can be accessed online at <https://doi.org/10.1080/10717544.2022.2149894>

© 2022 The Author(s). Published by Informa UK Limited, trading as Taylor & Francis Group.

This is an Open Access article distributed under the terms of the Creative Commons Attribution License (<http://creativecommons.org/licenses/by/4.0/>), which permits unrestricted use, distribution, and reproduction in any medium, provided the original work is properly cited.

2020; Liu et al., 2021), however, we should bear in mind, that since 2005, no oral nanocrystals was approved. This situation mainly caused by the limited bioavailability enhancing ability of nanocrystals as several researchers found that the bioavailability of some drugs could only be enhanced for less than 2-folds via nanocrystals (Liversidge & Conzentino, 1995; Mou et al., 2011). So, how to enlarge the oral bioavailability enhancing ability of nanocrystals has become a hot research field in nearly years. In recent years, researchers found that with the aid of functional polymer, the oral absorption of nanocrystals could be enhanced (Frank et al., 2015; Haeri et al., 2018). Excluding the enhancing ability on solubility and dissolution rate of nanocrystals, the bioavailability of polymer modified nanocrystals can further improved by enhanced endocytosis-mediated transport, paracellular pathways-introduced transport, M cell-mediated pathway-dependend transport, inhibition of P-gp efflux and so on (Mohammad et al., 2019; Mu et al., 2010; Song et al., 2022; Liu et al., 2018). Thus, developing multifunctional polymer modified nanocrystals may be a promising way for further bioavailability enhancement of poorly soluble drugs.

Many researchers have used either physical mixed multi-functional materials or synthesized copolymer to enlarge the oral absorption enhancing ability of nanocrystals (Ahuja et al., 2015; Qiao et al., 2017; Yi et al., 2015), however, whether the functional materials have played their full enhancing ability in oral absorption, or whether physical mixture of multiple functional materials and copolymer insisted with these materials play the same role on oral absorption enhancement is still unknown. To my best knowledge, due to the different physicochemical properties of nanocrystals and functional materials, the drug nanocrystals modified by a single polymer or a physical mixture of multiple polymers made separated in gastrointestinal tract and cannot reach the same site of gastrointestinal tract at the same time, hence limited the absorption enhancing ability of functional materials.

In this study, we intend to study the real-time distribution of drug and modified materials in gastrointestinal tract by labeling these materials with different fluorescent probes, and operated on a small animal live imaging system. The model functionals materials we selected were: (1) sodium dodecyl sulfate, which could open the tight junction between cells (Bezrodnykhet al., 2021), (2) chitosan, which could increase contact time with mucous membranes via its bio-adhesive behavior (Zoya et al., 2021; Chen et al., 2020; Liu et al., 2020), (3) D- $\alpha$ -Tocopherol polyethylene glycol 1000 succinate, a P-gp efflux inhibitor (Chen et al., 2021; Rathod et al., 2021).

## 2. Materials and methods

### 2.1. Materials

Sodium dodecyl sulfate (SDS), sodium chloride, ethyl acetate, dichloromethane and methanol were purchased from Xilong Scientific Chemical Reagent Co., Ltd, China. D- $\alpha$ -Tocopherol polyethylene glycol 1000 succinate (TPGS), chitosan (CS),

hydrochloric acid (HCl), triethylamine (TEA), succinic anhydride (SA) and 1-Ethyl-3-(3-dimethylaminopropyl) carbodiimide hydrochloride (EDC-HCl) was purchased from Aladdin, China. 4-dimethylaminopyridine (DMAP) was purchased from Energy Chemical, China. Andrographolide (purity > 98%) was purchased from Shanxi Tengmai Biotechnology co., Ltd, China. N-Hydroxysul fosuccinimide sodium salt (NHS) and 2-morpholinoethanesulfonic acid were purchased from Macklin, China. Arachidonic acid was purchased from Shanghai Kaiwei Chemical Technology Co., Ltd, China. Indomethacin was purchased from Shanghai Macklin Biochemical Technology Co., Ltd, China. Mouse TNF- $\alpha$  ELISA kit, mouse IL-1 $\beta$  ELISA kit and mouse IL-6 ELISA kit were purchased from Shanghai Jianglai Biotechnology Co., Ltd, China. HPLC-grade methanol was used for high performance liquid chromatography (HPLC). Acridine orange and fluorescein isothiocyanate isomer were purchased from Rhawn, China. Rhodamine B was purchased from Solarbio, China. All other materials and reagents were of analytical grade and purified water was used throughout this study.

Male Sprague Dawley (SD) rats, weighing 240-260 g and male mouse, weighing 25-30 g were supplied by Hunan SJA Laboratory Animal Co., Ltd, China.

### 2.2. Synthesis and characterization of SDS-CS-TPGS copolymer

The synthesis of SDS-CS-TPGS copolymer included four primary steps (Figure 1): (1) SDS acidification reaction: Adding SDS to methanol, and adding enough hydrochloric acid gas until the SDS methanol solution become clear, and then the SDS acidifier was obtained after removing methanol by rotary evaporation; (2) The synthesis of SDS-CS polymer: First, weighing 3.4 g CS and add it into 250 mL round-bottled flask, and then 100 mL water and 20 mL hydrochloric acid solution (5.0 mL  $\rightarrow$  100 mL) were added to dissolve CS. Second, mixing 7 mL 0.23 mM dimethyl aminopyridine ethanol solution and 7 mL 0.27 mM acidified SDS aqueous solution, and then reacted at 80  $^{\circ}$ C for 24 hours under the protection of nitrogen. Finally, the reaction product was centrifuged after cooled it to room temperature, and the supernatant was dialyzed by water and 50% ethanol solution for 4 h in triple and the SDS-CS was obtained by rotary evaporation and freeze-drying, thereafter; (3) The activation of TPGS (Chen et al., 2018): Weighing a certain amount of TPGS and succinic anhydride with molar ratio of 1:1.2, and mixed them with DMAP in a round-bottomed flask. After drying in a vacuum drying oven for 4 hours, these materials were dissolved by purified dichloromethane, and then reaction were operated by adding anhydrous triethylamine, and heating to reflux and stirring in an oil bath for 24 hours under nitrogen protection, and the viscous liquid TPGS succinate monoester was gained by purified with chloromethane-ethyl acetate-methanol solution (the ratio =9:2:2) and silica gel column. The TPGS succinic acid monoester was condensed with EDC-HCl and NHS, briefly: Weighing TPGS-COOH, EDC-HCl, and NHS in a molar ratio of 1: 1.2: 1.2, then dissolving TPGS-COOH and EDC-HCl with morpholine ethanesulfonic acid buffer (pH = 5.0), stirring

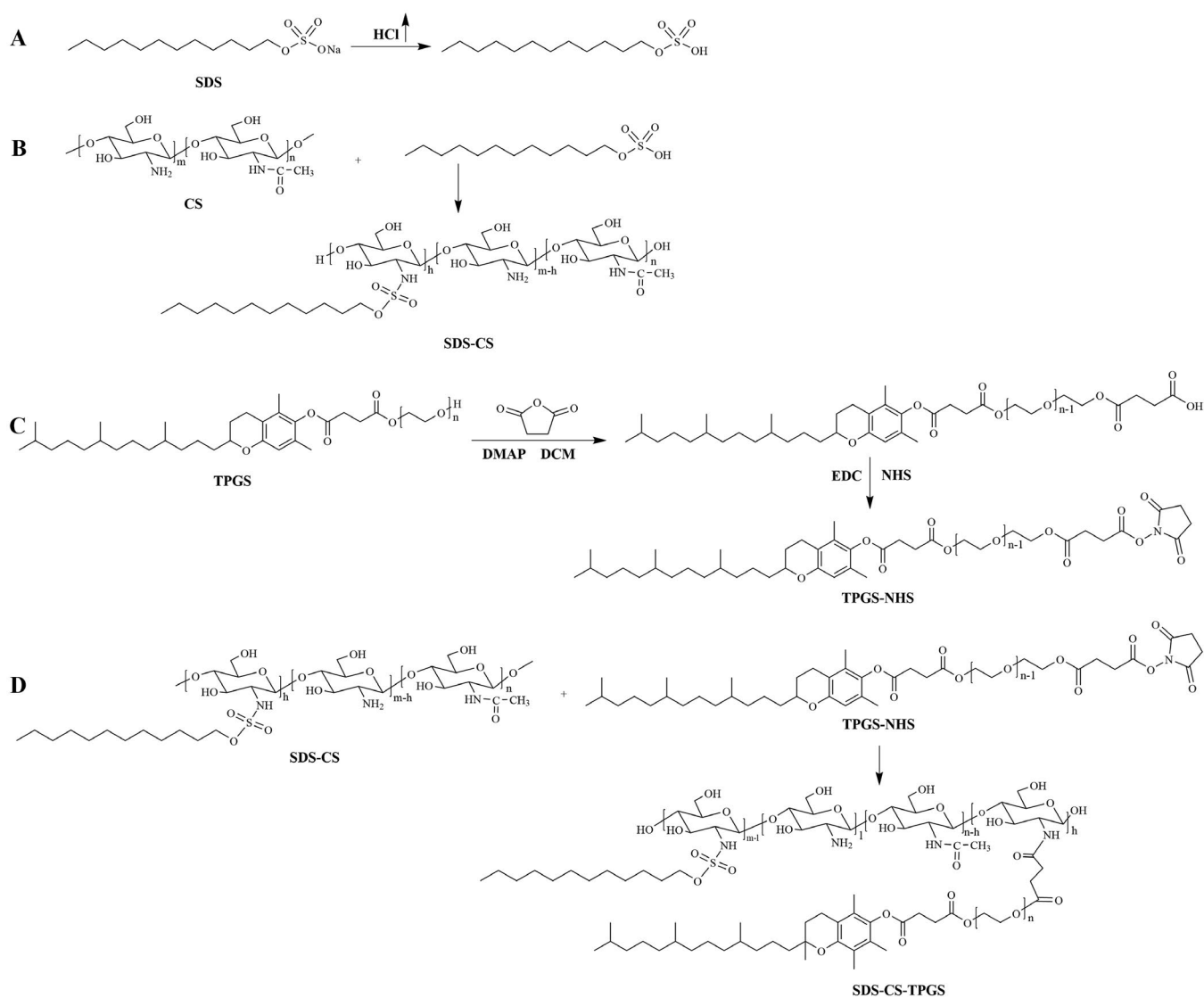


**Figure 1.** The synthesis process (A) of the SDS-CS-TPGS copolymer.

in an ice bath for 10 min, then reacting at room temperature for 6 hours); (4) The synthesis of SDS-CS-TPGS copolymer: SDS-CS and activated TPGS was dissolved by water, and reacted at room temperature for 24 hours. The SDS-CS-TPGS copolymer was gained after purified with dialysis bag and dried by freeze-dryer. The structure of new synthesized copolymers was confirmed by using  $^1\text{H}$  NMR and FT-IR spectroscopy.

### 2.3. Preparation of the nanocrystals

#### 2.3.1. Preparation of andrographolide nanocrystals (ANs)

Andrographolide nanocrystals (ANs) were prepared by high pressure homogenization. Firstly, andrographolide was dispersed in 50 mL purified water and pretreated by high shear homogenizer at 13000 rpm for 10 min using Fluko<sup>®</sup> FA25 (FLUKO, Germany). Secondly, the crude suspension was homogenized by high pressure homogenization machine (AH-NANO, ATS, China) with optimized parameters of 50 bar

for 2 cycles, 200 bar for 2 cycles, 500 bar for 2 cycles, 1000 bar for 20 cycles, with homogenization temperature of 41–50 °C.

#### 2.3.2. Preparation of stabilizer modified andrographolide nanocrystals (SANs, TANs and S-C-TANs)

Sodium dodecyl sulfate modified andrographolide nanocrystals (SANs) were prepared by high pressure homogenization with optimized parameters. Briefly, 250 mg andrographolide and 70.8 mg SDS were weighed and dispersed in 50 mL purified water. After high shear homogenization at 13,000 rpm for 10 min using Fluko<sup>®</sup> FA25, the suspension was homogenized by high pressure homogenizer with homogenization pressure of with optimized parameters of ANs. D- $\alpha$ -Tocopherol polyethylene glycol 1000 succinate modified andrographolide nanocrystals (TANs) was prepared by high pressure homogenization with optimized parameters of ANs. Briefly, 429.2 mg TPGS were weighed and dispersed in 50 mL purified water. After high shear homogenization at 13,000 rpm for 10 min using Fluko<sup>®</sup> FA25, the suspension was homogenized by high

pressure homogenizer with optimized parameters of ANs. The SDS-CS-TPGS copolymer modified andrographolide nanocrystals (S-C-TANs) was prepared by high pressure homogenization with optimized parameters of ANs. Briefly, 250 mg andrographolide and 500 mg SDS-CS-TPGS were weighed and dispersed in 50 mL purified water. After high shear homogenization at 13,000 rpm for 10 min, the suspension was homogenized with optimized parameters of ANs.

#### 2.4. Characterization of nanocrystals

The characterization of ANs, SANs, TANs and S-C-TANs was performed as below:

After the sample concentration was diluted to 0.1 mg/mL (calculated as andrographolide), the particle sizes, polydispersity indices (PDI) and zeta potentials of ANs, SANs, TANs and S-C-TANs were characterized with Nano ZS 90 nanoparticle sizer (Malvern Instruments Co., Ltd., UK), and all samples were analyzed in triplicate.

The morphology of andrographolide was performed on a scanning electron microscope (SEM) (quanta 250, Fei, America), while the morphology of ANs, SANs, TANs and S-C-TANs was analyzed on a transmission electron microscope (TEM) (Tecnai spirit, Fei America).

The crystalline states of ANs, SANs, TANs and S-C-TANs were studied by employing x-ray diffraction (XRD) (D/max 2500 PC, Japan Science Co., Ltd., Japan).

#### 2.5. Saturated solubility study

The saturation solubility of ADR was studied in hydrochloric acid aqueous solution (HCl, pH 1.2), citrate - disodium hydrogen phosphate buffer (C-DHPB, pH 4.0), phosphate buffered saline (PBS, pH 6.8) and purified water, respectively, at 37°C, while the saturation solubility of SDS and ADR physical mixture (SDS+ADR), TPGS and ADR physical mixture (TPGS+ADR) were studied in purified water at 37°C. Briefly, excess formulation powders were added into 5 mL buffers, and shaken at 37°C for 24 h, then the undissolved drug was removed by centrifuging at 13,000 rpm for 10 min and filtering with 0.22 µm microporous membrane. The drug concentration in the filtrate was determined by HPLC. The freshly prepared ANs, SANs, TANs and S-C-TANs were directly shaking for 24 h at 37°C, and treated as that of andrographolide, thereafter. ADR was analyzed at 225 nm and at 35°C using HPLC linked to Ultimate® XB-C18 (4.6 mm × 250 mm, 5 µm) column. The mobile phase which consisted of methanol and water (60:40, v/v) was pumped at 1 mL/min. The HPLC analysis met the methodological requirements by validating.

#### 2.6. Pharmacokinetic study

We explored oral absorption enhancing ability of andrographolide nanocrystals by operating pharmacokinetic studies on SD rat. In brief, twenty-five SD rats were randomly divided into 5 groups, and administrated ADR-water (dispersed ADR in water), ANs, SANs, TANs and S-C-TANs at 50 mg/kg by gavage (Chen et al., 2014). After administrated for 0.083,

0.25, 0.5, 0.75, 1, 2, 4, 6, 8, 12 and 24 h, about 0.3 mL blood sample was collected by retro-orbital puncture. The plasma was centrifuged at 4,000 r/min for 10 min at 4°C and stored at -20°C. The andrographolide concentrations in plasma samples were detected after treatments as following: 50 µL plasma samples, 25 µL luteolin solution (internal standard 10.11 µg/mL) and 200 µL methanol solution were mixed by vortexing for 5 min. The mixed solution was subsequently centrifuged at 12,000 rpm for 10 min and the supernatant was collected and dried at room temperature under a stream of nitrogen. The residue was reconstituted with 50 µL methanol and mixed by vortexing for 3 min. After centrifuging at 12,000 rpm for 10 min, the supernatant was injected into the HPLC system for analysis. The ADR concentration in plasma samples was detected by HPLC following the conditions shown in [supplementary materials](#), and pharmacokinetic parameters were calculated using the DAS 3.3.0 pharmacokinetics program (developed by the Clinical Trial Center of Shanghai University of Traditional Chinese Medicine, Shanghai, China).

#### 2.7. Real-time distribution of nanocrystals in the gastrointestinal tract

We performed real-time distribution study to explore whether the functional materials have played their full enhancing ability in oral absorption. We used acridine orange to label SDS, fluorescein isothiocyanate isomer I to label TPGS, CS, SDS-TPGS and SDS-CS-TPGS, and rhodamine B to label ADR, respectively. After labeling the samples, seventy-two SD rats were randomly divided into 6 groups, named SDS group, TPGS group, ADR group, CS group, SDS-CS-TPGS group and SDS-CS-TPGS+ADR group. The SDS-CS-TPGS+ADR group was administered with SDS-CS-TPGS and ADR at the same time. The animals were killed by cervical dislocation at the pre-set time points of 0.5 h, 1 h, 2 h and 3 h. Then the gastrointestinal tract was removed in time and put it into a small animal live imaging system (Lumina XR, PerkinElmer, America) for photographic observation.

#### 2.8. Study on anti-inflammatory effect of S-C-TANs

To explore whether the enhancing on bioavailability could result in enhanced therapeutic effect, we studied the anti-inflammatory efficacy of nanocrystal. The ear swelling ICR mice model was established by using arachidonic acid and the anti-inflammatory efficacy was evaluated by employing ear swelling rate of ICR mice serum levels of TNF-α, IL-6 and IL-1β, as pharmacodynamic index. In this study, fifty-six ICR mice were randomly divided into 8 groups, named control group (normal animal), model group (without drug), indomethacin group (positive drug, 10 mg/kg, po), ADR injection group (10 mg/kg, iv), ADR group (100 mg/kg, po), L-S-C-TANs group (low dose of S-C-TANs, 25 mg/kg, po), M-S-C-TANs group (middle dose of S-C-TANs, 50 mg/kg, po) and H-S-C-TANs group (high dose of S-C-TANs, 100 mg/kg, po). After treated with different drugs for 4 days, 25 µL arachidonic acid solution (200 mg/mL) was smeared on the right



ear of ICR mice, and after administrated for 0.5h, the serum was taken, and stored at  $-20^{\circ}\text{C}$  for detection of TNF- $\alpha$ , IL-1 $\beta$  and IL-6. Ears were cut off along the auricle baseline, and samples were taken from the same part of the left and right ears of the mice with an ear punch with diameter of 8mm. After the samples were taken and weighed, the swelling degree was indicated by the weight difference between the left and right ears. Cellular inflammatory factors, like TNF- $\alpha$ , IL-1 $\beta$ , and IL-6, were measured by Elisa Kit.

## 2.9. Statistical analysis

All values were expressed as the means  $\pm$  SD. The statistical analysis was performed using one-way ANOVA with SPSS Statistics 22.0 (SPSS Inc., Chicago, America). The differences were considered significant at  $p < 0.05$ .

## 3. Results and discussion

### 3.1. Synthesis of SDS-TPGS copolymer

The synthesized SDS-CS-TPGS copolymer was identified by  $^1\text{H}$  NMR and FT-IR. As shown in Figure 2A, the structure of SDS-CS-TPGS contains the hydrogen peaks of 'a' ( $\delta$  0.7 3 ~ 1.432 ppm), 'b' ( $\delta$  1.970 ppm), 'c' quartet ( $\delta$  2.520 ppm, 2.526 ppm, 2.537, 2.549 ppm), 'd' ( $\delta$  2.927 ppm), 'f' (quartet peak,  $\delta$  2.374 ppm, 2.385 ppm, 2.396 ppm, 2.410 ppm), 'q' ( $\delta$  2.927 ppm), 'j' (doublet peak,  $\delta$  3.606, 3.619 ppm), 'e' (doublet peak,  $\delta$  3.669, 3.687 ppm), 'k' (doublet peak,  $\delta$  3.734, 3.752 ppm), 'p' (doublet peak,  $\delta$  3.847, 3.868 ppm), 'g' (quartet peak,  $\delta$  4.177 ppm, 4.182 ppm, 4.184 ppm, 4.192 ppm), 'r' (solvent peak,  $\delta$  4.701 ppm), and these peaks could belong to SDS, CS or TPGS, indicating the  $^1\text{H}$  NMR spectrum was consistent with the theoretical  $^1\text{H}$  NMR spectrum of SDS-CS-TPGS.

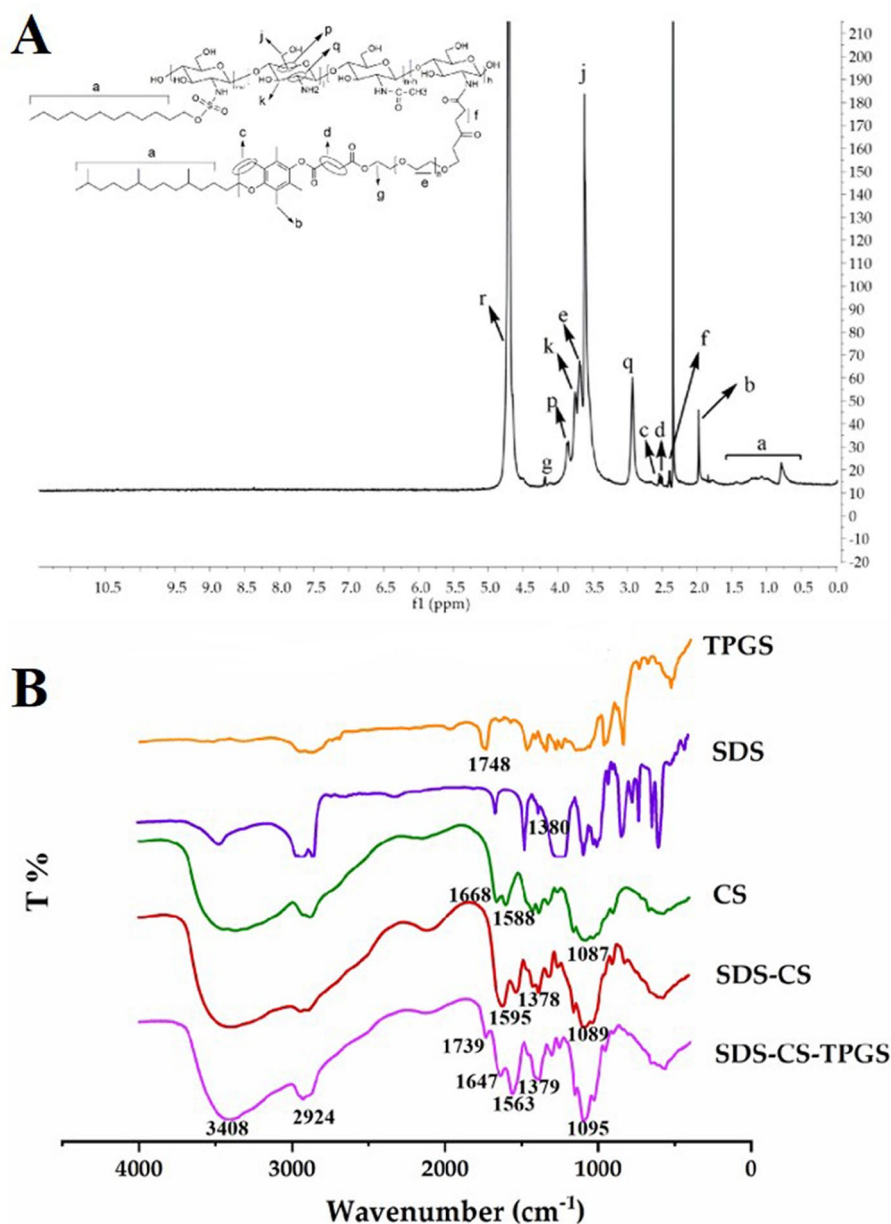


Figure 2. The  $^1\text{H}$  NMR spectra (B) and FT-IR spectra (C) of the SDS-CS-TPGS copolymer.

Then, we confirmed the results gained from  $^1\text{H}$  NMR by investigating the FI-TR profiles of different materials. Briefly, dry potassium bromide was mixed with SDS, TPGS, CS, SDS-CS and SDS-CS-TPGS, respectively, in a suitable proportion, and then the samples were pressed and tested by FI-TR to obtain the infrared spectrograms (Figure 2B). The special infrared peak of TPGS and SDS was 'C=O' ( $1748\text{ cm}^{-1}$ ) and 'S=O' ( $1380\text{ cm}^{-1}$ ), respectively, and CS exhibited special infrared peaks like 'C=O' ( $1588\text{ cm}^{-1}$ ), 'N-H' ( $1668\text{ cm}^{-1}$ ) and 'C-O-C' ( $1087\text{ cm}^{-1}$ ). In the spectra of SDS-CS, the 'C=O' ( $1595\text{ cm}^{-1}$ ), 'S=O' ( $1378\text{ cm}^{-1}$ ) and 'C-O-C' ( $1089\text{ cm}^{-1}$ ) existed, while the 'N-H' ( $1668\text{ cm}^{-1}$ ) was missing, indicating the acidified SDS could react with CS to form SDS-CS. The special infrared peaks in the SDS-CS-TPGS were 'C=O' ( $1739\text{ cm}^{-1}$ ) 'C=O' ( $1647\text{ cm}^{-1}$ ) 'N-H' ( $1563\text{ cm}^{-1}$ ) 'S=O' ( $1379\text{ cm}^{-1}$ ) 'C-O-C' ( $1095\text{ cm}^{-1}$ ) and 'C=O' ( $1739\text{ cm}^{-1}$ ), indicating that TPGS was connected to the SDS-CS, and the SDS-CS-TPGS copolymer was successfully synthesized.

### 3.2. Characterization of nanocrystals

In order to explore the oral absorption enhancing ability of SDS-CS-TPGS copolymer and nanocrystals, we prepared several kinds of nanocrystals: stabilizer-free andrographolide nanocrystals (ANs), SDS modified andrographolide nanocrystals (SANs), TPGS modified andrographolide nanocrystals (TANs) and SDS-CS-TPGS modified andrographolide nanocrystals (S-C-TANs), by high-pressure homogenization, and the production process was provided in [supplementary materials](#). Then these nanocrystals were characterized by Nano ZS 90 nanoparticle sizer (Malvern Instruments Co., Ltd., UK), transmission electron microscopy (TEM (Tecni spirit, Fei America)), X-ray diffraction (XRD (D/max 2500 PC, Japan Science Co., Ltd., Japan), etc.

The appearance of fresh prepared ADR-Water, ANs, SANs, TANs and S-C-TANs were shown in Figure 3(A), ANs, SANs, TANs and S-C-TANs were milky white suspension, while ADR-Water that has obvious large particles and was easy

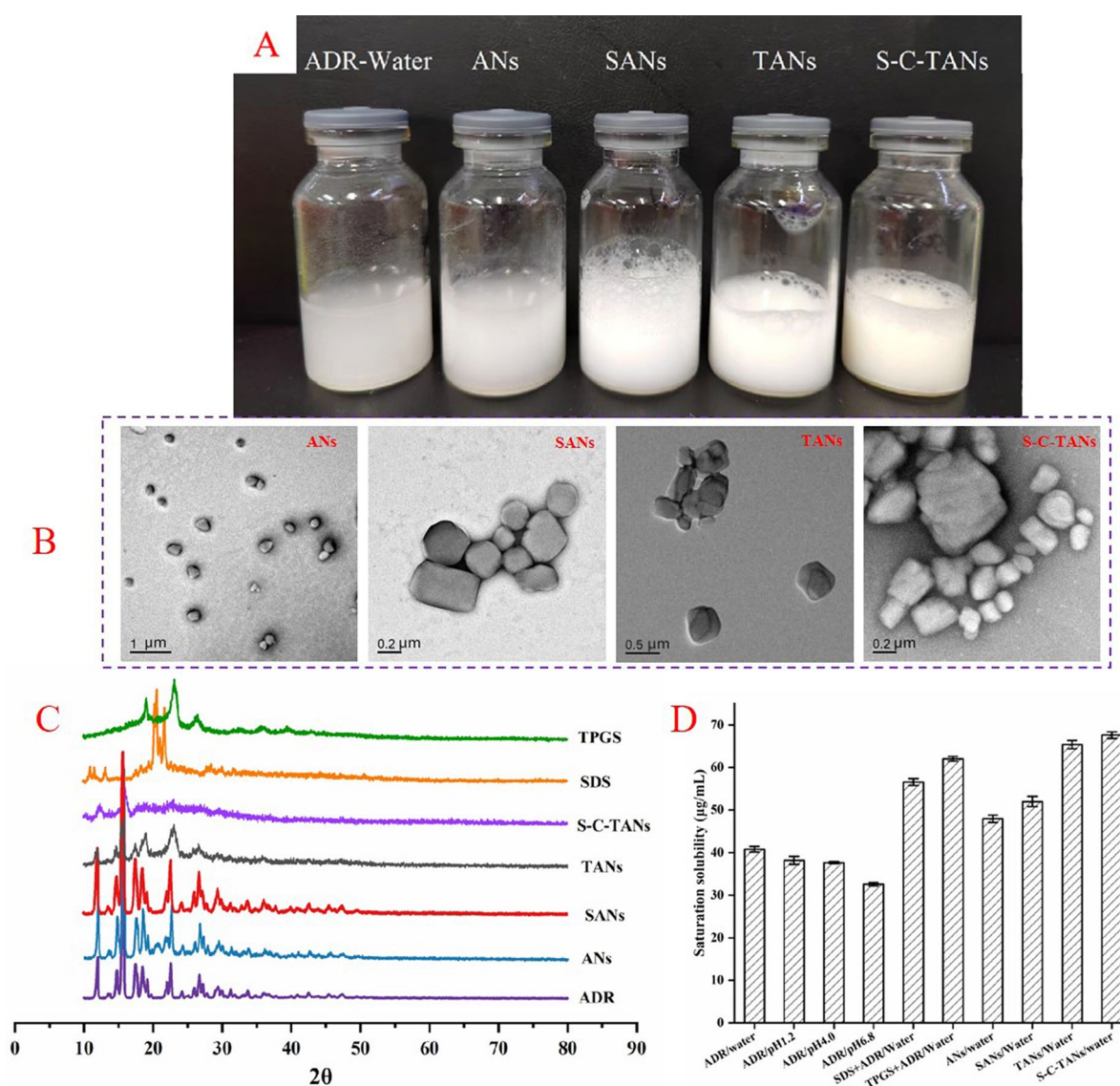


Figure 3. The appearance (A), TEM paragraph (B), XRD spectra (C) and saturation solubility (D) of andrographolide nanocrystals.

to settle and stratify. The particle sizes of ANs, SANs, TANS and S-C-TANs were  $368.3 \pm 4.7$  nm,  $506.1 \pm 8.1$  nm,  $552.5 \pm 4.9$  nm and  $573.2 \pm 3.9$  nm, respectively. That PDI values were above 0.3 indicate high heterogeneity, while the PDI of ANs, SANs, TANS and S-C-TANs were  $0.207 \pm 0.021$ ,  $0.191 \pm 0.017$ ,  $0.106 \pm 0.089$  and  $0.223 \pm 0.024$ . PDI values of those nanocrystals were all below 0.3, indicating the distribution of these nanocrystals were relatively uniform (Imam et al., 2015). It could be seen from the TEM spectra that the appearance of ANs liked a melon seed shell, while the SANs, TANS, and S-C-TANs were irregular spherical-liked (Figure 3B).

The crystalline states of ADR, SDS, TPGS, ANs, SANs, TANS and S-C-TANs were studied by employing x-ray diffraction (XRD) (Ultima IV, Rigaku, Tokyo, Japan). The XRD patterns of ADR, SDS, TPGS, ANs, SANs, TANS and S-C-TANs were depicted in Figure 3(C). The characteristic peaks of ADR presented at  $2\theta = 11.91^\circ, 14.68^\circ, 15.44^\circ, 17.46^\circ, 18.44^\circ, 19.22^\circ, 22.61^\circ, 24.40^\circ, 26.68^\circ, 27.26^\circ, 29.54^\circ, 31.16^\circ, 33.77^\circ, 36.06^\circ, 40.90^\circ, 42.48^\circ$ , and the characteristic peaks of SDS presented at  $2\theta = 11.06^\circ,$

$11.66^\circ, 13.32^\circ, 20.62^\circ, 21.82^\circ$ , while the characteristic peaks of TPGS presented at  $2\theta = 19.06^\circ, 23.26^\circ, 26.26^\circ$ . It could be seen from the paragraphs that the diffraction peaks of ANs and SANs are roughly the same as those of ADR, indicating the crystalline form of nanocrystals has not changed under high pressure homogenization or modified by SDS. The characteristic peaks of TANS presented at  $2\theta = 11.91^\circ, 15.44^\circ, 17.46^\circ, 19.12^\circ, 23.26^\circ, \text{ and } 26.46^\circ$ , and the diffraction peaks became less and weaker, showing the TANS was partly transformed from crystal state to amorphous state. excluding the peaks at  $2\theta$  were  $12.31^\circ$  and  $15.88^\circ$ , there was no other diffraction peak in the XRD spectra of S-C-TANs, indicating the nanocrystals were nearly in amorphous.

### 3.3. The saturation solubility of andrographolide and nanocrystals

Figure 3(D) exhibited the saturation solubilities of ADR and its nanocrystals, and the results showed with the increasing of pH, the saturation solubility of ADR decreased. The

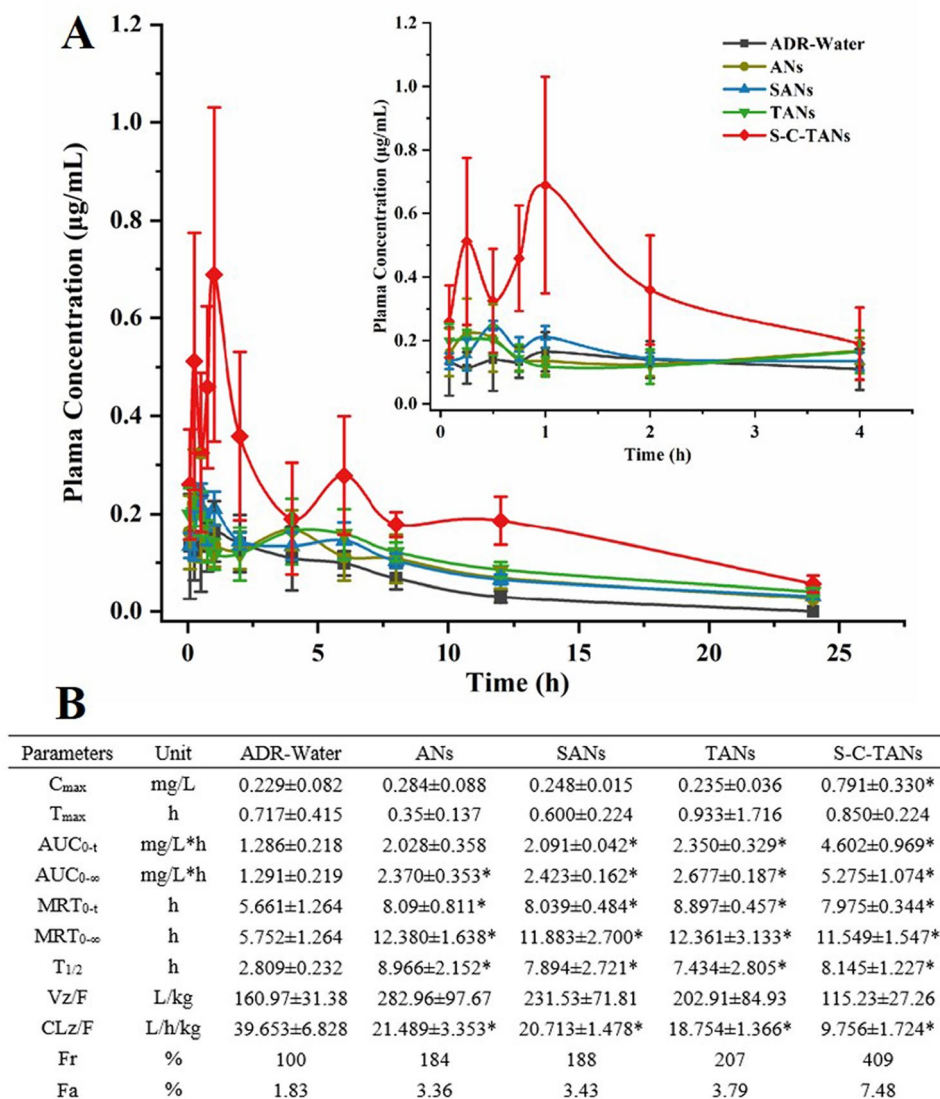


Figure 4. The pharmacokinetic curves (A) and parameters (B) andrographolide nanocrystals (mean  $\pm$  SD,  $n = 5$ ).



saturation solubility of ADR in water at 37 °C was  $40.79 \pm 0.64 \mu\text{g/mL}$ , and after transformed the ADR into nanocrystals, the solubility was slightly increased for about 1.17-folds (shown in Table S1). The saturated solubility of nanocrystals was further increased after being modified by functional materials.

### 3.4. Pharmacokinetic study

We explored oral absorption enhancing ability of andrographolide nanocrystals by operating pharmacokinetic studies on SD rat. The pharmacokinetic behaviors of ADR, ANs, SANs, TANs and S-C-TANs are shown in Figure 4. Compared with the ADR-Water group, the  $\text{AUC}_{0-\infty}$  of the ANs increased from  $1.291 \text{ mg/L}\cdot\text{h}$  to  $2.370 \text{ mg/L}\cdot\text{h}$ , indicating nanocrystals could significantly increase the oral absorption of andrographolide. After modified with SDS or TPGS, no significant change happened on  $C_{\text{max}}$  of nanocrystals, while the  $\text{AUC}_{0-\infty}$  was slightly increased. After modified with SDS-CS-TPGS copolymer, nanocrystals gained the highest  $C_{\text{max}}$  and bioavailability. The  $C_{\text{max}}$  was enhanced from  $0.284 \pm 0.088 \mu\text{g/mL}$  for ANs to  $0.791 \pm 0.330 \mu\text{g/mL}$  for S-C-TANs. Compared with ADR-Water, the relative bioavailability of ANs, SANs, TANs, and S-C-TANs were 184%, 188%, 207%, 240%, 297%, and 409%, respectively, and the absolute bioavailability of andrographolide (ADR) and S-C-TANs was 1.83% and 7.48%, respectively. The pharmacokinetic study of ADR-Water and ANs showed that nanocrystal technology could significantly improve the oral bioavailability of ADR, and the comparison of the pharmacokinetic parameters of SANs, TANs and ANs showed that the modification of drug nanocrystals by functional materials can further improve the oral bioavailability of andrographolide. Among these functional materials, the SDS-CS-TPGS

copolymer, formed by chemical synthesis of different functional materials showed the highest ability on enhancing oral bioavailability of andrographolide. The first peak in pharmacokinetic curves is caused by the absorption of drug, while the peak emerged at about 6 h is caused by the enterohepatic circulation (Guan & Morris 2019).

### 3.5. Real-time distribution in the gastrointestinal tract

The distribution of gastrointestinal segments in each group of animals at each time period was observed by in live imaging system (Figure 5A). We could know that the fluorescence intensity of each group decreases as time went on, and we could preliminarily see that the distribution of SDS, CS and TPGS in the gastrointestinal tract of SD rats was different from the distribution of ADR, while the distribution of SDS-CS-TPGS in the gastrointestinal tract is roughly the same as the distribution of ADR, when SDS-CS-TPGS and ADR were administered at the same time. In order to further understand the distribution of various materials and ADR in the gastrointestinal tract, we divided the gastrointestinal tract of SD rats into ten parts such as stomach, small intestine which divided into 8 sections on average and colon, as shown in Figure 5(B). The Figure 5(C) and Table S2 (in supplementary materials) showed the fluorescence intensity statistics of the distribution of polymer materials and ADR in various parts of the gastrointestinal tract, which can more intuitively reflect that the time of the site was close that they reached the same level in the gastrointestinal tract of SD rats when SDS-CS-TPGS and ADR are administered at the same time. For example, when SDS-CS-TPGS were taken orally with ADR, the time of 50% SDS-CS-TPGS passing part 4, part 5 and part 6 of small intestine was  $0.67 \pm 0.01 \text{ h}$ ,  $0.98 \pm 0.06 \text{ h}$  and

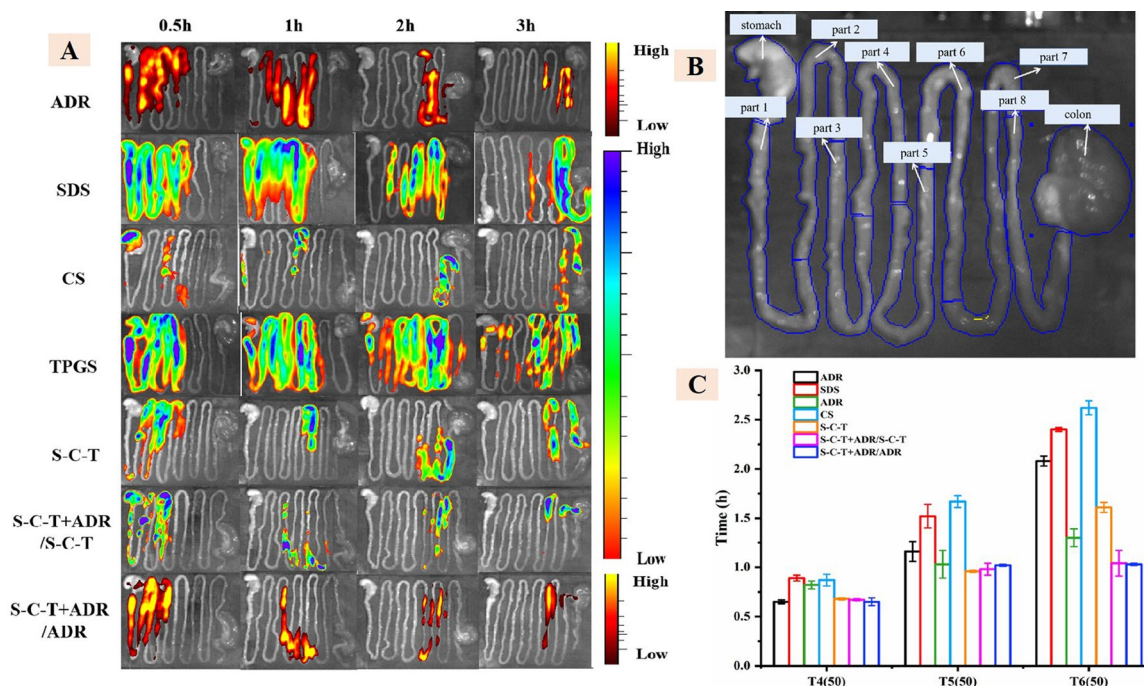


**Figure 5.** The real-time distribution (A), gastrointestinal segments (B) and passing time(C) of 50% materials through the fourth, fifth and sixth segments of small intestine (mean  $\pm$  SD,  $n=3$ ).



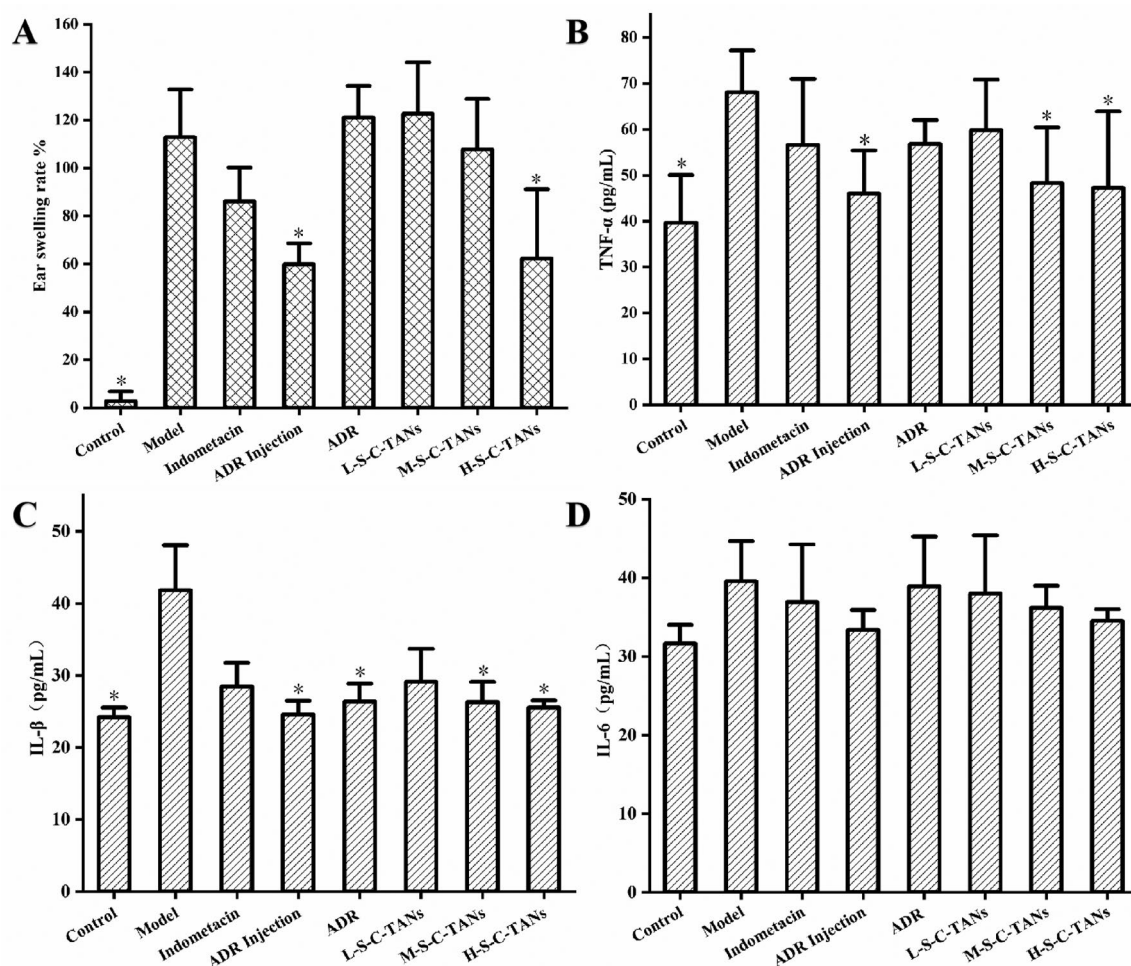


**Figure 6.** The effect of nanocrystals on ear swelling rate (A), TNF- $\alpha$  (B), IL-1 $\beta$  (C) and IL-6 (D) in mice (mean  $\pm$  SD,  $n=7$ , \* $P<0.05$  vs. model group).

1.04  $\pm$  0.13 h, respectively, which were not much different from that of ADR, as the passing time of ADR in part 4, part 5 and part 6 was 0.65  $\pm$  0.04 h, 1.02  $\pm$  0.01 h and 1.03  $\pm$  0.01 h, respectively. However, these times of other materials and ADR were different, indicating the materials and ADR could not reach the same site of gastrointestinal tract at the same time, which may limit the absorption enhancing ability of functional materials. Combining the results described above, we can conclude that materials in physical mixture may separate in intestinal, and synthesized copolymer could reduce the separation and has better ability to research the absorption site of drug at the same time.

### 3.6. The anti-inflammatory effect of S-C-TANs

To explore whether the enhancing on bioavailability could result in enhanced therapeutic effect, we studied the anti-inflammatory efficacy of nanocrystal. The ear swelling ICR mice model was established by using arachidonic acid and the anti-inflammatory efficacy was evaluated by employing ear swelling rate of ICR mice serum levels of TNF- $\alpha$ , IL-6 and IL-1 $\beta$ , as pharmacodynamic index. In this study, fifty-six ICR mice were randomly divided into 8 groups, named control group (normal animal), model group (without drug),

indomethacin group (positive drug, 10 mg/kg, po), ADR injection group (10 mg/kg, iv), ADR group (100 mg/kg, po), L-S-C-TANs group (low dose of S-C-TANs, 25 mg/kg, po), M-S-C-TANs group (middle dose of S-C-TANs, 50 mg/kg, po) and H-S-C-TANs group (high dose of S-C-TANs, 100 mg/kg, po). After treated with different drugs for 4 days, 25  $\mu$ L arachidonic acid solution (200 mg/mL) was smeared on the right ear of ICR mice, and the ears and blood samples were harvested after 0.5 h.

The ear swelling ICR mice model was successfully established as there were significant difference on pharmacodynamic index between model group and control group (Figure 6). Comparing the treatment groups, we could find that the ear swelling rate of the mice in the injection group and the H-S-C-TANs group decreased significantly (Figure 6A). The anti-ear swelling efficacy of all groups were as follow: ADR injection group > H-S-C-TANs group > positive drug group > M-S-C-TANs group > ADR group  $\approx$  L-S-C-TANs group. The effects of nanocrystals on cellular inflammatory factors TNF- $\alpha$ , IL-1 $\beta$  and IL-6 in ear swelling mice were shown in Figure 6(B)-D. Compared with the control group, the values of TNF- $\alpha$  and IL-1 $\beta$  in the model group changed significantly, indicating the model stimulated TNF- $\alpha$  and IL-1 $\beta$  in mice, while the IL-6 factor showed no significant difference between the all groups, indicating the model did not stimulate the

changes of IL-6 cell inflammatory factors in mice. From the results of TNF- $\alpha$  and IL-1 $\beta$  studies, there were significant differences between the model group and the ADR injection group, M-S-C-TANs group and H-S-C-TANs group, and the TNF- $\alpha$  and IL-1 $\beta$  levels of H-S-C-TANs group were similar to that of ADR injection group. The above results indicated the enhanced bioavailability could lead to enhanced pharmacodynamic effect, and SDS-CS-TPGS modified nanocrystals (100 mg/kg) have the similar anti-inflammatory efficacy with ADR injection (10 mg/kg).

#### 4. Conclusion

In this study, we employed three different functional stabilizers to synthesize multifunctional SDS-CS-TPGS copolymer and used this copolymer to modify the andrographolide nanocrystals (S-C-TANs). The particle size and zeta potential of S-C-TANs was  $573.2 \pm 3.9$  nm and  $46.27 \pm 0.25$  mV, and the saturation solubility of andrographolide was increased for about 1.7-folds by nanocrystals. With the aids of increased solubility and absorption enhancing efficacy of SDS-CS-TPGS, the  $C_{max}$  and  $AUC_{0-\infty}$  of andrographolide was enhanced from  $0.229 \pm 0.082$  mg/L,  $1.291 \pm 0.219$  mg/L\*h to  $0.791 \pm 0.330$  mg/L and  $5.275 \pm 1.074$  mg/L\*h, respectively. In addition, we confirmed the synthesized SDS-CS-TPGS copolymer could increase the absorption enhancing potential of multiple functional materials by maintaining the similar distribution behaviors of drug and materials in gastrointestinal tract. The enhanced bioavailability leads to enhanced anti-inflammatory efficacy of nanocrystals by performing on arachidonic acid induced inflammation ICR mice model. This study indicated that modified with synthesized copolymer containing different functional stabilizers is an efficient strategy to enlarge the enhancing ability on oral absorption of nanocrystals.

#### Data availability statement

The data that support the findings of this study are available from the corresponding author, L. Tu, upon reasonable request.

#### Disclosure statement

No potential conflict of interest was reported by the authors.

#### Ethical approval statement

The study was conducted according to the guidelines of the Declaration of Helsinki, and approved by the Institutional Review Board of Jiangxi University of Chinese Medicine (protocol code: JZLLSC20220361).

#### Funding

This work was supported by the National Natural Science Foundation of China (81960717), the Jiangxi University of Chinese Medicine science and technology innovation team development program (CXTD-22008, CXTD-22004), the '1050' Young Talent Scholar discipline project of Jiangxi University of Chinese Medicine (5142001012) and the PhD startup foundation of Jiangxi University of TCM (2018BSZR018).

#### References

- Ahuja BK, Jena SK, Paidi SK, et al. (2015). Formulation, optimization and in vitro–in vivo evaluation of febuxostat nanosuspension. *Int J Pharm* 478:540–52.
- Basu A, Gutti S, Kundu S, et al. (2020). Oral andrographolide nanocrystals protect liver from paracetamol induced injury in mice. *J Drug Deliv Sci Tech* 55:101406.
- Bezrodnykh EA, Antonov YA, Berezin BB, et al. (2021). Molecular features of the interaction and antimicrobial activity of chitosan in a solution containing sodium dodecyl sulfate. *Carbohydr Polym* 270:118352.
- Casamonti M, Risaliti L, Vanti G, et al. (2019). Andrographolide loaded in micro- and nano-formulations: improved bioavailability, target-tissue distribution, and efficacy of the “king of bitters”. *Engineering* 5:69–75.
- Chellampillai B, Pawar AP. (2011). Improved bioavailability of orally administered andrographolide from pH-sensitive nanoparticles. *Eur J Drug Metab Pharmacokinet* 35:123–9.
- Chen HW, Huang CS, Li CC, et al. (2014). Bioavailability of andrographolide and protection against carbon tetrachloride-induced oxidative damage in rats. *Toxicol Appl Pharmacol* 280:1–9.
- Chen TE, Tu L, Wang G, et al. (2020). Multi-functional chitosan polymeric micelles as oral paclitaxel delivery systems for enhanced bioavailability and anti-tumor efficacy. *Int J Pharm* 578:119105.
- Chen TE, Wang G, Chen MT, et al. (2018). Preparation of TPGS-chitosan-loaded paclitaxel micelles and in vivo intestinal absorption in rats. *Chin Tradit Herbal Drugs* 49:5780–6.
- Chen Y, Gui Y, Luo Y, et al. (2021). Design and evaluation of inhalable nanocrystals embedded microparticles with enhanced redispersibility and bioavailability for breviscapine. *Powder Technol* 377:128–38.
- Cheng M, Yuan F, Liu J, et al. (2020). Fabrication of fine puerarin nanocrystals by Box–Behnken Design to enhance intestinal absorption. *AAPS PharmSciTech* 21:1–12.
- Frank LA, Contri RV, Beck RCR, et al. (2015). Improving drug biological effects by encapsulation into polymeric nanocapsules. *Wiley Interdiscip Rev Nanomed Nanobiotechnol* 7:623–39.
- Guan XW, Morris ME. (2019). Pharmacokinetics of the monocarboxylate transporter 1 inhibitor AZD3965 in mice: potential enterohepatic circulation and target-mediated disposition. *Pharm Res* 37:5.
- Haeri A, Osouli M, Bayat F, et al. (2018). Nanomedicine approaches for sirolimus delivery: a review of pharmaceutical properties and preclinical studies. *Artif Cells Nanomed Biotechnol* 46:1–14.
- He G, Yan X, Miao ZH, et al. (2020). Anti-inflammatory catecholic chitosan hydrogel for rapid surgical trauma healing and subsequent prevention of tumor recurrence. *Chin Chem Lett* 31:1807–11.
- Hussain RT, Islam AKMS, Khairuddean M, et al. (2022). A polypyrrole/GO/ZnO nanocomposite modified pencil graphite electrode for the determination of andrographolide in aqueous samples. *Alex Eng J* 61:4209–18.
- Imam SS, Aqil M, Akhtar M, et al. (2015). Formulation by design-based proniosome for accentuated transdermal delivery of risperidone: in vitro characterization and in vivo pharmacokinetic study. *Drug Deliv* 22:1059–70.
- Kesisoglou F, Panmai S, Wu Y. (2007). Nanosizing—oral formulation development and biopharmaceutical evaluation. *Adv Drug Deliv Rev* 59:631–44.
- Khan I, Khan F, Farooqui A, et al. (2018). Andrographolide exhibits anticancer potential against human colon cancer cells by inducing cell cycle arrest and programmed cell death via augmentation of intracellular reactive oxygen species level. *Nutr Cancer* 70:787–803.
- Latif R, Wang CY. (2020). Andrographolide as a potent and promising antiviral agent. *Chin J Nat Medicines* 18:760–9.
- Li L, Li S, Jiang J, et al. (2021). Investigating pharmacological mechanisms of andrographolide on non-alcoholic steatohepatitis (NASH): a bioinformatics approach of network pharmacology. *Chin Herb Med* 13:342–50.
- Lim JCW, Sagineedu SR, Yong ACH, et al. (2021). Toxicological and pharmacokinetic analysis at therapeutic dose of SRS27, an investigational

- anti-asthma agent. *Naunyn-Schmiedeberg's Arch Pharmacol* 394:95–105.
- Liu D, Wan B, Qi J, et al. (2018). Permeation into but not across the cornea: bioimaging of intact nanoemulsions and nanosuspensions using aggregation-caused quenching probes. *Chin Chem Lett* 29:1834–8.
- Liu JL, Sun YB, Cheng M, et al. (2021). Improving oral bioavailability of luteolin nanocrystals by surface modification of sodium dodecyl sulfate. *AAPS PharmSciTech* 22:133.
- Liu JL, Tu L, Cheng M, et al. (2020). Mechanisms for oral absorption enhancement of drugs by nanocrystals. *J Drug Deliv Sci Tech* 56:101607.
- Liu Q, Cheng M, Liang J, et al. (2020). Enhancing oral bioavailability by paclitaxel polymeric micelles: Role of transmembrane pathways in the oral absorption. *J Biomed Nanotechnol* 16:1160–8.
- Liversidge GG, Conzentino P. (1995). Drug particle size reduction for decreasing gastric irritancy and enhancing absorption of naproxen in rats. *Int J Pharm* 125:309–13.
- Lu Y, Chen Y, Gemeinhart RA, et al. (2015). Developing nanocrystals for cancer treatment. *Nanomedicine (Lond.)* 10:2537–52.
- Magar KT, Boafu GF, Zoulikha M, et al. (2023). Metal phenolic network-stabilized nanocrystals of andrographolide to alleviate macrophage-mediated inflammation in-vitro. *Chin Chem Lett* 34:107453.
- Marta C, Laura R, Giulia V, et al. (2019). Andrographolide loaded in micro- and nano-formulations: improved bioavailability, target-tissue distribution, and efficacy of the “King of Bitters”. *Engineering* 5:69–75.
- Methenitis S, Stergiou I, Antonopoulou S, et al. (2021). Can exercise-induced muscle damage be a good model for the investigation of the anti-inflammatory properties of diet in humans? *Biomedicines* 9:36.
- Mohammad IS, Hu HY, Yin LF, He W. (2019). Drug nanocrystals: fabrication methods and promising therapeutic applications. *Int J Pharm* 562:187–202.
- Mou DS, Chen HB, Wan JL, et al. (2011). Potent dried drug nanosuspensions for oral bioavailability enhancement of poorly soluble drugs with pH-dependent solubility. *Int J Pharm* 413:237–44.
- Mu CF, Balakrishnan P, Fu-De C, et al. (2010). The effects of mixed MPEG-PLA/pluronic copolymer micelles on the bioavailability and multidrug resistance of docetaxel. *Biomaterials* 31:2371–9.
- Parveen R, Ahmad FJ, Iqbal Z, et al. (2014). Solid lipid nanoparticles of anticancer drug andrographolide: formulation, in vitro and in vivo studies. *Drug Dev Ind Pharm* 40:1206–12.
- Qiao Z, Chen LH, Rui TQ, et al. (2017). Fabrication and in vitro/in vivo evaluation of amorphous andrographolide nanosuspensions stabilized by D- $\alpha$ -tocopheryl polyethylene glycol 1000 succinate/sodium lauryl sulfate. *Int J Nanomedicine* 12:1033–46.
- Rathod S, Bahadur P, Tiwari S. (2021). Nanocarriers based on vitamin E-TPGS: design principle and molecular insights into improving the efficacy of anticancer drugs. *Int J Pharm* 592:120045.
- Song Q, Wang H, Yang J, et al. (2022). A “cluster bomb” oral drug delivery system to sequentially overcome the multiple absorption barriers. *Chin Chem Lett* 33:1577–83.
- Tran QTN, Tan DWS, Wong WSF, et al. (2020). From irreversible to reversible covalent inhibitors: harnessing the andrographolide scaffold for anti-inflammatory action. *Eur J Med Chem* 204:112481.
- Tu L, Cheng M, Sun Y, et al. (2020). Fabrication of ultra-small nanocrystals by formation of hydrogen bonds: in vitro and in vivo evaluation. *Int J Pharm* 573:118730.
- Wang X, Liu J, Dai Z, et al. (2021). Andrographolide improves PCP-induced schizophrenia-like behaviors through blocking interaction between NRF2 and KEAP1. *J Pharmacol Sci* 147:9–17.
- Yi YN, Tu LX, Hu KL, et al. (2015). The construction of puerarin nanocrystals and its pharmacokinetic and in vivo–in vitro correlation (IVIVC) studies on beagle dog. *Colloids Surf B Biointerfaces* 133:164–70.
- Zafar A, Imam SS, Alruwaili NK, et al. (2021). Development of piperine-loaded solid self-nanoemulsifying drug delivery system: optimization, in-vitro, ex-vivo, and in-vivo evaluation. *Nanomaterials* 11:2920.
- Zhao S, Li J, Wang F, et al. (2020). Semi-elastic core-shell nanoparticles enhanced the oral bioavailability of peptide drugs. *Chin Chem Lett* 31:1147–52.
- Zhang H, Li S, Si Y, et al. (2021). Andrographolide and its derivatives: current achievements and future perspectives. *Eur J Med Chem* 224:113710.
- Zhang JM, Li YB, Gao W, et al. (2014). Andrographolide-loaded PLGA-PEG-PLGA micelles to improve its bioavailability and anticancer efficacy. *Expert Opin Drug Deliv* 11:1367–80.
- Zou LH, Ding WY, Huang QY, et al. (2022). Andrographolide/phospholipid/cyclodextrin complex-loaded nanoemulsion: preparation, optimization, in vitro and in vivo evaluation. *Biol Pharm Bull* 45:1106–15.
- Zoya I, He HS, Wang LT, et al. (2021). The intragastric fate of paclitaxel-loaded micelles: Implications on oral drug delivery. *Chin Chem Lett* 32:1545–9.